THE ASTROPHYSICAL JOURNAL, 428:713–728, 1994 June 20

HIGH-PRECISION TIMING OF MILLISECOND PULSARS. III. LONG-TERM MONITORING OF PSRs B1885+09 AND B1937+21

V. M. KASPI,[1] J. H. TAYLOR,[2] AND M. F. RYBA[3]
Joseph Henry Laboratories and Physics Department, Princeton University, Princeton, NJ 08544
Received 1993 August 19; accepted 1993 December 22

ABSTRACT

Biweekly timing observations of PSRs B1855+09 and B1937+21 have been made at the Arecibo Observatory for more than 7 and 8 yr, respectively, with uniform procedures and only a few modest gaps. On each observing date we measure an equivalent pulse arrival time for PSR B1855+09 at 1.4 GHz, with typical accuracies of about 0.8 μs, and for PSR B1937+21 at both 1.4 and 2.4 GHz, with accuracies around 0.2 μs. The pulse arrival times are fitted to a simple model for each pulsar, yielding high-precision astrometric, rotational, and orbital parameters, and a diverse range of conclusions. The celestial coordinates and proper motions of the two pulsars are determined with uncertainties ≤ 0.12 mas and ≤ 0.06 mas yr^{-1} in the reference frame of the DE200 planetary ephemeris. The annual parallaxes are found to be $\pi = 1.1 \pm 0.3$ mas and $\pi < 0.28$ mas for PSRs B1855+09 and B1937+21, respectively. The general relativistic Shapiro delay is measured in the PSR B1855+09 system and used to obtain masses $m_1 = 1.50^{+0.26}_{-0.14}\ M_\odot$ and $m_2 = 0.258^{+0.028}_{-0.016}\ M_\odot$ for the pulsar and its orbiting companion. The extremely stable orbital period of this system provides a phenomenological limit on the secular change of Newton's gravitational constant, $\dot{G}/G = (-9 \pm 18) \times 10^{-12}$ yr^{-1}. Variations in the dispersion measure of PSR B1937+21 indicate that the spectrum of electron-density fluctuations in the interstellar medium has a power-law index $\beta = 3.874 \pm 0.011$, slightly steeper than the Kolmogorov value of 11/3, and we find no strong evidence for an "inner scale" greater than about 2×10^9 cm.
2×10^9 cm.

In the residual pulse arrival times for PSR B1937+21 we have observed small systematic trends not explained by our deterministic timing model. We discuss a number of possible causes; although the results are not yet conclusive, the most straightforward interpretation is that the unmodeled noise (a few microseconds over 8 yr, or $\Delta t/T \approx 10^{-14}$) is inherent to the pulsar itself. In the present data set, PSR B1855+09 exhibits no discernible timing noise. With conventional assumptions we derive a limit $\Omega_g h^2 < 6 \times 10^{-8}$ (95% confidence) for the energy density, per logarithmic frequency interval, in a cosmic background of stochastic gravitational waves. We discuss the feasibility of establishing a pulsar-based timescale that might be used to test the stabilities of the best available atomic clocks. In an Appendix, we propose guidelines for the archiving of pulsar timing observations. Instructions are provided for obtaining copies of our own archival data, via Internet.

Subject headings: astrometry — binaries: close — gravitation — ISM: general — pulsars: individual (PSR B1855+09, PSR B1937+21)

1. INTRODUCTION

Timing observations of binary and millisecond pulsars can be highly accurate sources of a wide variety of astrophysical information. Earlier papers in this series (Ryba & Taylor 1991a, b; hereafter Papers I and II) described measurements of pulse arrival times for PSR B1855+09 and PSR B1957+20, obtained at the Arecibo Observatory between 1986 and 1990. PSR B1855+09 is a binary pulsar with a 5.4 ms period in a nearly circular, 12.3 day orbit. In Paper I, timing observations were used to measure its position, proper motion, and annual parallax, all at the sub-milliarcsecond level; in addition, the general relativistic orbital "Shapiro delay" was measured and used to determine the masses of the pulsar and its unseen companion, thought to be a white dwarf. PSR B1957+20 has a 1.6 ms period and is in a 9.2 hr eclipsing orbit around a low-mass companion apparently in the process of evaporating. Paper II presented a detailed study of this complex system including an accurate proper motion, a thorough description of its eclipse phenomenology, and a measured change of its orbital period.

These high-precision timing observations of fast-rotating pulsars are an outgrowth of a continuing series of measurements of the relativistic binary pulsar, PSR B1913+16, begun in 1974 (Taylor & Weisberg 1989, and references therein). Observations of PSR B1937+21, the fastest known pulsar, have been made on an approximately biweekly basis since late 1982 (Backer, Kulkarni, & Taylor 1983; Davis et al. 1985; Rawley et al. 1987; Rawley, Taylor, & Davis 1988; Stinebring et al. 1990). When PSR B1855+09 was discovered (Segelstein et al. 1986) it was added to the observing schedule as well, and recently there have been further additions. Our data-acquisition facilities for timing fast pulsars were substantially upgraded in 1984 (Rawley 1986), and again in 1989 (Ryba 1991; Stinebring et al. 1992), resulting in higher accuracy and better uniformity of the measurements. The observations continue at Arecibo on a regular schedule, usually twice per month.

In this paper we report the progress of this long and continuing experiment through the end of 1992, concentrating on the longest term and highest precision aspects of timing PSR B1855+09 and PSR B1937+21. Our data sets for these two

[1] e-mail: vicky@pulsar.princeton.edu.
[2] e-mail: joe@pulsar.princeton.edu.
[3] Present address: MIT Lincoln Laboratory, Lexington, MA 02173. e-mail: ryba@ll.mit.edu.

pulsars arguably represent the state of the art in pulsar timing. The continuous spans of regular, high-quality observations now exceed 7 and 8 yr, respectively, and measurements have been obtained on more than 150 distinct dates for each pulsar. Relativistic models with just nine free parameters (for PSR B1937+21) and 16 parameters (for PSR B1855+09) fit the data remarkably well, determining the astrometric and spin parameters, dispersion measures, and orbital elements, mostly with accuracies of 3–16 significant digits. The simple, deterministic timing models for the two pulsars account for all but a tiny fraction of the total "signal" contained in the timing observations. As an example, we note that the Earth's motion causes an annual variation in pulse arrival times with peak-to-peak amplitude nearly 10^3 s, and yet the post-fit timing residuals for the two pulsars have root mean square amplitudes around 10^{-6} s.

Although the residual pulse arrival times for PSR B1855+09 are essentially featureless when plotted as a function of date, those for PSR B1937+21 exhibit systematic trends indicative of unmodeled physical effects. By hypothetically attributing all such low-frequency noise to a cosmic background of graviational waves, one can obtain a reliable upper limit on the possible energy density in such radiation at frequencies around 10^{-8} Hz (Stinebring et al. 1990). We do not consider it likely that the observed trends in the timing residuals are, in fact, caused by gravity waves. We discuss at length various other possible causes of the low-frequency noise. Although the results are not yet conclusive, it appears likely that most of the irregularities seen in PSR B1937+21 are inherent to the pulsar itself.

The information content of high-precision pulsar timing observations like these argues forcefully that they should be continued and extended. For the results to be most useful it is essential that carefully measured pulse arrival times, traceable to the best available standards of atomic time, be archived for potential use many years from now. In an Appendix we propose some guidelines for the archival recording of pulse arrival times, and we describe a data base in which all measurements described in this paper now reside, freely accessible to anyone via Internet.

2. ARRIVAL TIME MEASUREMENTS

We describe results based on measurements made at the Arecibo Observatory through the end of 1992. Observations of PSR B1855+09 and/or PSR B1937+21 were obtained on 244 dates during this interval. The observing procedures and many significant features of the data-acquisition hardware were described in Papers I and II, so we shall summarize them only briefly here. Nearly all of the measurements of PSR B1855+09 have been made at frequencies close to 1408 MHz, where the Arecibo telescope provides an equivalent system noise of about 5 Jy in each sense of circular polarization. Between 1986 January and 1990 January, pulse times of arrival (TOAs) were obtained with the Princeton "Mark II" pulsar timing equipment (Rawley 1986; Rawley, Taylor, & Davis 1988), identified in Table 1 as observing system A. This system used a dual-polarization 32 × 0.25 MHz filter-bank spectrometer followed by 32 digital signal averagers, each synchronized with the predicted topocentric pulse period. Starting in 1989 January, we also used our "Mark III" pulsar timing system (Stinebring et al. 1992), which makes use of the same 0.25 MHz filter bank (observing system C) as well as another with wider bandwidths of 1.25 MHz per channel (system D). During each biweekly session we observed PSR B1855+09 for slightly less than an hour, usually obtaining about 25 independent 2 minute integrations. For 13 days during 1990 April, the observations were extended to over 2 hr per day in order to optimize the measureability of relativistic effects in the pulsar orbit. The data set for PSR B1855+09 analyzed here spans about 7 yr and exactly 40,879,349,533 rotations of the pulsar on its axis. The total number of daily-average TOAs collected for PSR B1855+09 with each observing system is listed in Table 1, together with their median estimated uncertainties. The span of dates for each of the data sets is illustrated schematically at the top of Figure 1.

The Mark II system was used for regular observations of PSR B1937+21 between 1984 October and 1989 July. Measurements were made in frequency bands near both 1408 MHz (system A) and 2380 MHz (system B); at the higher frequency, the equivalent system noise is about 6 Jy. Further details concerning these observations can be found in Rawley (1986), Rawley et al. (1987), and Rawley et al. (1988). Regular measurements of PSR B1937+21 with the Mark III system commenced in 1989 January at 1408 MHz, and in July of that year at 2380 MHz (Stinebring et al. 1990; Taylor 1991; Ryba 1991). In addition to system C these observations make use of system E, a four-channel coherent dedisperser spanning a pair of 1.25 MHz bands near 1408 MHz (Hankins, Stinebring & Rawley 1987; Ryba 1991), and system F, the dual 32 × 0.25 MHz filter bank at 2380 MHz. In each scheduled observing session we follow PSR B1937+21 at 1408 and 2380 MHz for approximately 30 and 50 minutes, respectively. At 1408 MHz, the wide-bandwidth filter bank is used to search the entire 40 MHz passband of the feed antenna for scintillation-induced signal maxima. The coherent dedispersers are automatically tuned to the frequencies of the best two maxima for the next 2 minute integration, while the narrow filter bank operates independently at fixed frequency. In the same way, results from the wide

TABLE 1

MEASURED TOAS AND MEDIAN UNCERTAINTIES, THROUGH 1992 DECEMBER

OBSERVING SYSTEM	FREQUENCY (MHz)	BANDWIDTH (MHz)	PSR B1855+09		PSR B1937+21	
			TOAs	σ (μs)	TOAs	σ (μs)
A. Mark II	1408	32 × 0.25	76	1.20	116	0.22
B. Mark II	2380	32 × 0.25	...	...	92	0.20
C. Mark III	1408	32 × 0.25	97	0.92	77	0.26
D. Mark III	1408	32 × 1.25	98	0.74	...	...
E. Mark III	1408	2 × 1.25[a]	...	...	82	0.18
F. Mark III	2380	32 × 0.25	...	...	73	0.19

[a] Dispersion removed coherently, before square-law detection.

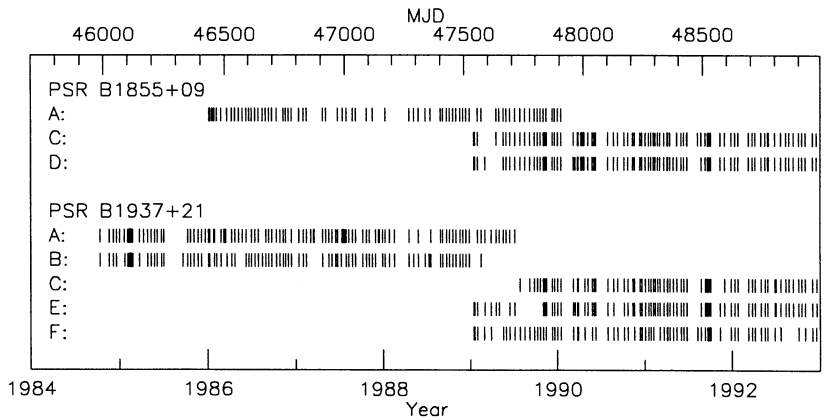

FIG. 1.—Schematic plot of the dates on which TOAs were obtained for PSRs B1855+09 and B1937+21. The Mark II data acquisition system was used for data sets A and B, and the Mark III system for the remainder. All TOAs were measured at frequencies near 1408 MHz, except for data sets B and F, at 2380 MHz.

filter bank are used to keep the narrow filter bank centered on a scintillation maximum during observations near 2380 MHz. Again the total number of daily-average TOAs and their median uncertainties are listed in Table 1 for each observing system, and the span of dates is indicated in Figure 1. The analyzed data set for this pulsar spans more than 8 yr and accounts for exactly 165,711,423,279 turns of the pulsar on its axis.

When the filter-bank spectrometers are in use, average total-intensity pulse profiles are recorded for each frequency channel together with a time stamp corresponding to the first data sample in a period near the middle of the integration. With the coherent dedispersers of observing system E, average profiles are recorded for each sense of circular polarization in each of two frequency channels. Pulse times of arrival are determined in the Fourier transform domain, by fitting the recorded profiles to a standard profile specific to the pulsar and the particular observing system (Taylor 1992). A single weighted-average TOA is finally computed for each pulsar, for each observing system, on each observing day. Examples of the standard profiles for PSRs B1855+09 and B1937+21 are shown in Figure 2.

A pulse TOA is a relativistic event and must be treated with careful attention to the measurement of all four space-time coordinates. Because the precisions of some observable parameters exceed the accuracy of the reference standards, results must be quoted in a clearly specified system of units, including definitions of the spatial reference frame and the atomic time scale. Following our previous practice (Stinebring et al. 1990), we adopt the widely distributed DE200 ephemeris of the Jet Propulsion Laboratory (Standish 1982) as our basic solar system model and the atomic timescale TT(BIPM92) (Guinot 1988) as our basic standard of terrestrial time. For comparison purposes we also use alternative timescales and ephemerides (see §§ 6.1, 6.2). Unpredictable variations in the rotation of the Earth affect the position of the telescope at the time of an observation, and we make suitable adjustments using data published in Bulletin B of the International Earth Rotation Service.

The time stamps recorded with our data are obtained from reference ticks generated by the Arecibo Observatory's master clock. Small drifts of this clock (generally of order 1 μs over a day or so) are monitored by means of transmissions from the Global Positioning System of satellites (GPS). With these measured offsets we correct TOAs retroactively to the timescale UTC(NIST), the version of Coordinated Universal Time maintained by the US National Institute of Standards and Technology. The accuracy of GPS in common-view mode assures that errors in the transfer of time from one location to another are negligible. Further corrections from UTC(NIST) to UTC, and then to TT(BIPM92) or some other highly stable realization of terrestrial time, are made by interpolating tables distributed by NIST and the Bureau International des Poids et Mesures (BIPM). The retrospective timescale TT(BIPM92) is intended to be the "world's best clock" in terms of long-term stability (Guinot 1988; Guinot & Petit 1990). New versions of TT(BIPM) are computed annually, using accumulated know-

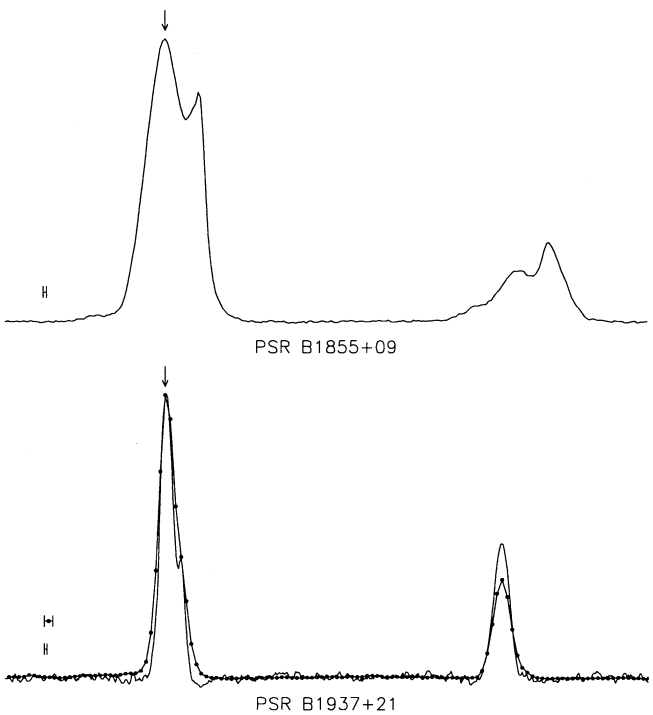

FIG. 2.—*Upper*: standard profile for PSR B1855+09 obtained with observing system C. The corresponding profile for system D is almost indistinguishable. *Lower*: standard profiles for PSR B1937+21, obtained with observing systems E (*solid line*) and F (*line with dots*). Instrumental smoothing is indicated by horizontal bars at the left of each plot, and arrows mark the phase of the nominal pulse arrival time.

ledge of the past performance of numerous atomic clocks around the world. Together these same clocks determine UTC, the standard kept in near real time and approximated, with varying degrees of accuracy, by civil time services.

3. TIMING MODEL

A comprehensive relativistic timing model for pulsars was described in Paper I, along with a detailed procedure for fitting the model to a sequence of pulse arrival times. Derivation of the model and some particulars of its implementation can be found in papers by Damour & Deruelle (1985, 1986), Taylor & Weisberg (1989), and Damour & Taylor (1992). Briefly, a one-to-one mapping is assumed between pulse phase within a recorded profile and the rotational phase of a spinning pulsar. The relevant physics is contained in equations describing gravitational interactions among massive bodies and electromagnetic signals in the solar system, similar gravitational interactions within a binary pulsar system, and a simple braking law describing the pulsar rotation itself. The essence of the model lies in the relativistic transformation between time coordinates t and T, measured respectively in the terrestrial frame and the comoving pulsar frame (ignoring a constant offset and a nearly constant and usually uninteresting Doppler factor—see Damour & Taylor 1991). The transformation is summarized by the equation

$$\begin{aligned} T = t - t_0 + \Delta_C - D/f^2 + \Delta_{R\odot}(\alpha, \delta, \mu_\alpha, \mu_\delta, \pi) \\ + \Delta_{E\odot} - \Delta_{S\odot}(\alpha, \delta) \\ - \Delta_R(x, e, P_b, T_0, \omega) - \Delta_E(\gamma) - \Delta_S(r, s) - \Delta_A , \end{aligned} \quad (1)$$

where t_0 is a reference epoch; Δ_C is the offset between the observatory master clock and the reference standard of terrestrial time; D/f^2 is the dispersive delay for propagation at frequency f through the interstellar medium; $\Delta_{R\odot}$, $\Delta_{E\odot}$, and $\Delta_{S\odot}$ are propagation delays and relativistic time adjustments for effects within the solar system; and Δ_R, Δ_E, Δ_S, and Δ_A are terms with similar purposes for effects within a binary pulsar's orbit.

In addition to their explicitly indicated dependences on model parameters, the various Δ's are also functions of time. Their subscripts indicate the nature of the additive time delays, which include "Roemer," "Einstein," and "Shapiro" effects within the solar system, and these as well as "Abberration" effects in the pulsar orbit. The Roemer terms have amplitudes given approximately by $(P_b/2\pi)(v/c)$, where P_b is the orbital period, v a speed characteristic of orbital motion, and c the speed of light. The Einstein terms are smaller by another power of (v/c), multiplied by the orbital eccentricity. In the solar system, the term $\Delta_{E\odot}$ defines a clock rate offset determined by an arbitrary choice of time interval over which to subtract the mean value of $d\Delta_{E\odot}/dt$ (Taylor & Weisberg 1989). This procedure effectively defines the barycentric unit of time. In our standard fits we evaluate $\Delta_{E\odot}$ from the semianalytical model of Fairhead, Bretagnon, & Lestrade (1988). The one-way Shapiro delay $\Delta_{S\odot}$ in the solar system has a maximum variation of about 120 μs between solar conjunction and opposition, its functional form depending logarithmically on the impact parameter of the line of sight past the Sun (Shapiro 1964). The corresponding delay in a binary pulsar orbit depends on the companion star's mass, the orbital phase, and the inclination i between the orbital angular momentum and the line of sight from Earth to pulsar. Full details on all of the terms appearing in equation (1) can be found in the references quoted earlier.

Once the transformation described by equation (1) has been carried out, the pulsar rotational phase (in cycles) at the time of pulse emission can be computed from

$$\phi(T) = \phi_0 + \nu T + \tfrac{1}{2}\dot{\nu} T^2 , \quad (2)$$

where ϕ_0 is the phase at $T = 0$, ν the pulsar spin frequency, and $\dot{\nu}$ its first time derivative. As described in Paper I, model fitting is accomplished by adjusting the parameters ϕ_0, ν, $\dot{\nu}$, D, α, δ, etc., to minimize the weighted sum of squared differences between computed values of ϕ and the nearest integers. The pulsar period $P \equiv 1/\nu$ and its derivative $\dot{P} \equiv -\dot{\nu}/\nu^2$ are conventionally quoted in tables in place of ν and $\dot{\nu}$; similarly, observers generally use a dispersion measure defined by $\mathrm{DM} = (2.410 \times 10^{-16}\ \mathrm{cm}^{-3}\ \mathrm{pc\ s})D$, with D in Hz. We choose to set $\phi_0 = 0$ and to quote instead $t_\oplus$, an equivalent geocentric pulse arrival time for which the fractional part of $\phi(T)$ is exactly zero. A geocentric reference epoch $t_\oplus$ at a specified frequency $f_\oplus$ has the advantage of removing observatory site-specific details from an archival record of the zero point of pulsar phase, without introducing other uncertainties related to a particular solar system ephemeris or a poorly known dispersion measure.

We have written equations (1) and (2) to show explicitly the nature of the most significant dependences of TOAs on potentially measurable pulsar parameters. In addition to the rotational parameters $t_\oplus$, ν, and $\dot{\nu}$, these include the dispersion constant D, celestial coordinates α and δ, proper motion components $\mu_\alpha \equiv \dot{\alpha}\cos\delta$ and $\mu_\delta \equiv \dot{\delta}$, and annual parallax π. The last four terms in equation (1) are relevant only for binary pulsars; they permit the measurement of five Keplerian parameters of the orbital motion, including the projected semimajor axis $x \equiv a_1 \sin i/c$, eccentricity e, binary period P_b, time of periastron T_0, and longitude of periastron ω. If the experimental timing precision is high enough, relativistic effects give access to additional, "post-Keplerian" measurables (Damour & Taylor 1992). For our present data set on PSR B1855+09, only two such quantities are measurably nonzero: r and s, the "range" and "shape" of the Shapiro delay in the binary system. They are involved in an orbital phase-dependent delay that is closely approximated, for small orbital eccentricities, by

$$\Delta_S = -2r \ln\{1 - s\cos[2\pi(\varphi - \varphi_0)]\} , \quad (3)$$

where φ is the orbital phase in cycles and φ_0 is the phase of superior conjunction. Together with the five Keplerian parameters, the fitted values of r and s suffice for determining the masses of the pulsar and its orbiting companion within a specified relativistic theory of gravity—as we do in § 8.2 below.

4. DISPERSION MEASURE OF PSR B1937+21

Previous observations have shown that the dispersion measure of PSR B1937+21 varies significantly over time (Rawley et al. 1988; Cordes et al. 1990). For this reason we regularly measure its TOAs at two widely spaced frequencies, 1408 and 2380 MHz. Figure 3 illustrates the values of DM obtained from timing observations made since 1984 October. Each plotted point represents an observing date on which reliable TOAs were obtained at both frequencies. Incremental dispersion measures were computed from the relation

$$\Delta\mathrm{DM} = (2.410 \times 10^{-16}\ \mathrm{cm}^{-3}\ \mathrm{pc\ s})\left(\frac{\phi_2 - \phi_1}{\nu}\right)\left(\frac{1}{f_2^2} - \frac{1}{f_1^2}\right)^{-1} , \quad (4)$$

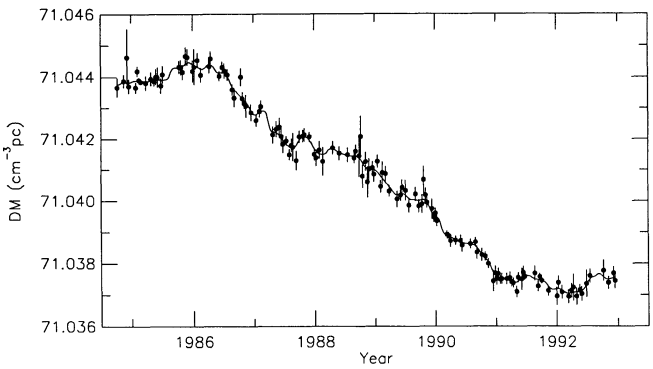

FIG. 3.—Dispersion measure of PSR B1937+21 plotted as a function of time. The smooth curve is a Gaussian-weighted running mean of the measurements, and is used in the most accurate timing solutions.

where ϕ_1 and ϕ_2 are the computed pulsar phases for TOAs obtained at barycentric frequencies f_1 and f_2. Because the pulse shape of PSR B1937+21 depends weakly on frequency, alignment of the standard profiles is necessarily somewhat arbitrary (see Fig. 2). Our chosen alignment biases the computed dispersion measures by a small amount, probably on the order of ± 0.002 cm^{-3} pc. The observed *variations* in DM are, of course, unaffected by such bias as long as it remains constant. Over our 8.2 yr data set, the changes in DM for PSR B1937+21 amount to a roughly monotonic fractional decrease of about one part in 10^4.

Following Rawley et al. (1988), we smooth the DM changes by computing a Gaussian-weighted running mean with full-width at half-maximum 55 days, and weights truncated to zero beyond ± 110 days. The resulting smoothed curve, plotted for reference in Figure 3, is used in place of D in equation (1) when making the highest precision fits to pulse arrival times for PSR B1937+21. Since the DM of PSR B1855+09 is more than 5 times smaller than that of PSR B1937+21, and the measurement uncertainties several times larger, it is very unlikely that any DM changes would be significant (see also Phillips & Wolszczan 1991). Therefore, we have not tried to measure them.

5. TIMING PARAMETERS

Fitted timing parameters for the two pulsars are presented in Table 2. Our basic solution for PSR B1937+21 includes five astrometric quantities, the dispersion measure, and three rotational parameters, $t_\oplus$, ν, and $\dot{\nu}$. The same nine quantities plus seven orbital parameters are needed to fit the data for PSR B1855+09. For all fitted parameters except the post-Keplerian quantities r and s, the curvature of the goodness-of-fit statistic χ^2 is nearly constant over its relevant cross sections near the global minimum. The parameter uncertainty ranges are therefore symmetric and have their customary interpretations in terms of confidence intervals (1 σ = 68%, 2 σ = 95%, etc.). In order to obtain the best possible estimates of acceptable ranges of r and s, we followed the same procedure used in Paper I and made a full two-dimensional map of $\chi^2(r, s)$ near its minimum. Contours from this map enclosing 68%, 95%, and 99.73% confidence regions are plotted in Figure 4. The results for r and s listed in Table 2 correspond to the innermost of these contours.

As partial tests of completeness of the timing model, we include in Table 2 the values of several extra parameters, namely $\ddot{\nu}$, $\dot{\omega}$, $\dot{x}$, $\dot{e}$, and $\dot{P}_b$, measured by allowing one at a time to

TABLE 2

TIMING PARAMETERS FOR PSRS B1885+09 AND B1937+21

Parameter	PSR B1855+09	PSR B1937+21
α (J2000)	$18^h57^m36^s.393520(5)$	$19^h39^m38^s.560210(2)$
δ (J2000)	09°43′17″.32346(12)	21°34′59″.14166(6)
μ_α (mas yr^{-1})	−2.94(4)	−0.130(8)
μ_δ (mas yr^{-1})	−5.41(6)	−0.464(9)
π (mas)	1.1(3)	0.12(8)
DM (cm^{-3} pc)	13.309(5)	71.040[a]
$t_\oplus$ (MJD)	47526.000000067884[b]	47500.000000015133[b]
$f_\oplus$ (MHz)	1408.0	2380.0
P (ms)	5.36210045404154(3)	1.557806468819794(2)
$\dot{P}$ (10^{-20})	1.78363(8)	10.51193(2)
ν (Hz)	186.4940816702299(10)	641.9282626022265(8)
$\dot{\nu}$ (10^{-16} s^{-2})	−6.2035(3)	−433.1671(8)
$\ddot{\nu}$ (10^{-27} s^{-3})	-1.0 ± 0.9[c]	13.2 ± 0.3[c]
x (s)	9.2307802(4)	...
e	0.00002168(5)	...
P_b (s)	1065067.59086(5)	...
ω	276°.41(9)[d]	...
T_0 (MJD)	47529.897(3)[d]	...
r (μs)	$1.27^{+0.14}_{-0.08}$	...
s	$0.9992^{+0.0004}_{-0.0007}$	...
$\dot{\omega}$ (yr^{-1})	$0°.03 \pm 0°.04$[c]	...
$\dot{x}$ (10^{-15})	-0.9 ± 2.1[c]	...
$\dot{e}$ (10^{-15} s^{-1})	0.0 ± 0.5[c]	...
$\dot{P}_b$ (10^{-12})	0.6 ± 1.2[c]	...

NOTE.—Figures in parentheses represent uncertainties in the last digits quoted and do not include uncertainties in the reference standards (see text).

[a] Dispersion measure of PSR B1937+21 varies (see Fig. 3).

[b] Experimental uncertainties in $t_\oplus$ are not relevant; they are necessarily dominated by our somewhat arbitrary phasing of the standard profiles.

[c] These parameters set equal to zero when calculating the other parameters and the residuals plotted in Fig. 5. The listed values were obtained by allowing one extra parameter at a time to vary.

[d] Parameters ω and T_0 are highly covariant. Observers should use ω = 276°.410 and T_0 = 47529.8971482.

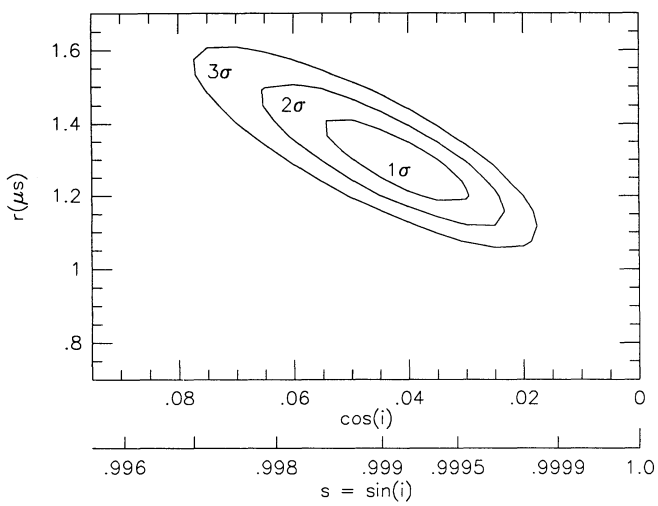

FIG. 4.—Contours delimiting the nominal 1 σ, 2 σ, and 3 σ confidence intervals for the post-Keplerian parameters r and s in the PSR B1855+09 system.

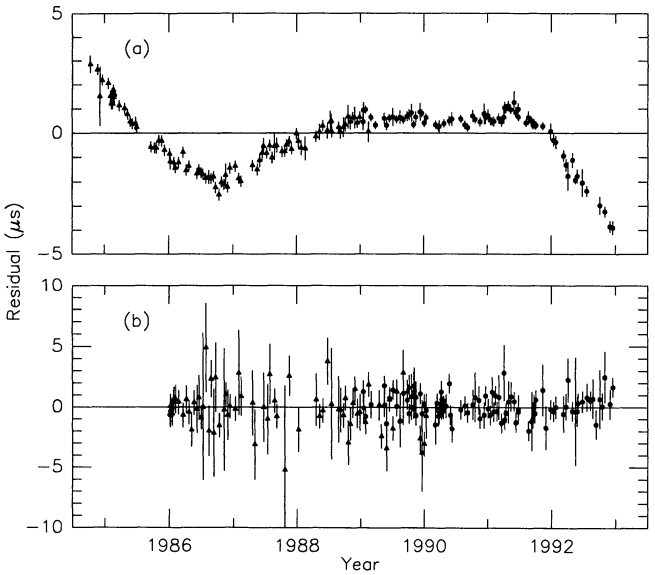

FIG. 5.—Timing residuals for (*a*) PSR B1937+21 and (*b*) PSR B1855+09, relative to the parameters listed in Table 2 (with $\ddot{\nu} = \dot{\omega} = \dot{x} = \dot{e} = \dot{P}_b = 0$). For clarity we have included only the highest quality data: for PSR B1937+21, the DM-corrected TOAs obtained at 2380 MHz with observing systems B (*triangles*) and F (*filled circles*), and for PSR B1855+09, those obtained at 1408 MHz with observing systems A (*triangles*) and D (*filled circles*).

vary in the fit. In general their values are consistent with zero; however, the nonzero second derivative $\ddot{\nu}$ for PSR B1937+21 is the tell-tale sign of slowly varying, unmodeled timing noise. Figure 5 illustrates the timing residuals for both pulsars, relative to the parameters in Table 2, with all of the extra parameters set to zero. The residuals for PSR B1937+21 show obvious systematic trends at the level of a few microseconds. To emphasize that this unmodeled noise is actually *very* small, we point out that 2 μs over 3 yr represents a fractional error of 2×10^{-14}—just about equal to the estimated long-term stability of the best atomic clocks. Because no comparable variations are seen in the residuals for PSR B1855+09, we believe that at most a minor portion of the low-frequency noise in the PSR B1937+21 residuals can be ascribed to any source common to both pulsars.

Whatever the source of unidentified fluctuations, to prevent them from biasing the fitted parameter values (especially the astrometric quantities) we proceeded as follows. First, enough additional spin-down derivatives $\ddot{\nu}$, $\dddot{\nu}$, etc., were added (by extending the Taylor series in eq. [2]) to fully "whiten" the appearance of the postfit residuals. Two frequency derivatives were sufficient for PSR B1855+09, while seven were required for PSR B1937+21. The resulting solutions yielded the astrometric and orbital parameters listed in Table 2. With these quantities held fixed and the extra derivatives reset to zero, another solution yielded the basic rotational parameters $t_\oplus$, ν, and $\dot{\nu}$. Finally, the values listed for $\ddot{\nu}$ and secular derivatives of orbital elements were obtained by allowing variation of one of these quantities at a time, along with the remaining parameters in Table 2.

Celestial coordinates are given for equinox J2000 in the fundamental reference frame of the DE200 ephemeris. As mentioned in § 2, our barycentric units of time are based on the retrospective timescale TT(BIPM92) and the relativistic transformation of Fairhead et al. (1988). The listed parameter uncertainties are larger (by factors of 1.1–3) than the formal standard errors determined by least-squares fitting; they are intended to represent 68% confidence limits, including both random and systematic errors, within the stated coordinate system and reference timescale. The uncertainties do *not* allow for possible errors in the reference standards; we discuss these separately in § 6. All tabulated parameters are consistent with those published in Paper I, and most of the uncertainties have been significantly reduced. In the DE200 reference frame, the position of PSR B1855+09 is now determined to about 0.1 mas and the proper motion to about 0.06 mas yr^{-1}. The corresponding accuracies for PSR B1937+21 are nearly 10 times better, approaching the microarcsecond level.

6. POSSIBLE SOURCES OF TIMING NOISE

Figure 5 shows that our TOAs for PSR B1937+21 are contaminated by one or more sources of unmodeled noise, well in excess of the measurement errors. The same is not true for PSR B1855+09, however. Deviations from the timing models at levels of a few microseconds over many years, equivalent to fractional instabilities of a few parts in 10^{14}, are hardly surprising: we are unaware of *any* clock comparison experiments that can boast significantly smaller residual differences over similar time intervals. The observed low-frequency noise in the PSR B1937+21 data set is very real, and its ultimate source has not previously been identifiable. In this section we consider the five sources of systematic timing noise generally thought to be the most plausible contributors in this experiment: ephemeris errors, atomic clock instabilities, changes in interstellar propagation times, rotational irregularities in the pulsar itself, and a cosmic gravitational wave background. Because comparable sequences of TOAs now exist for two different pulsars, we can begin to discriminate between sources of noise producing common-mode errors and those generating uncorrelated deviations.

6.1. *Solar System Ephemeris Errors*

The timing solutions presented in § 5 are based on the DE200 ephemeris and the timescale TT(BIPM92). Other choices of reference standards are possible, with at least partial independence from the chosen ones. Some aspects of the possible dependence of timing residuals on the solar system model and the timescale can therefore be tested by direct comparisons. To this end we have carried out independent solutions similar to those described earlier, but using a different ephemeris or timescale. For alternative solar system models we used PEP740R, developed and maintained at the Harvard-Smithsonian Center for Astrophysics (CfA) and DE211, an experimental version of the Jet Propulsion Laboratory (JPL) ephemeris that takes advantage of recent data from the 1988 *Voyager* encounter with Neptune (see Standish 1993). The three solar system models are not fully independent, as they are based in large part on the same sources of astronomical data. Nevertheless, the detailed implementations of the CfA and JPL models are quite different (for example, in the way they accommodate the minor planets), and differences between their respective timing solutions for pulsars should be instructive.

Table 3 lists the differences $\Delta\alpha$, $\Delta\delta$, $\Delta\mu_\alpha$, $\Delta\mu_\delta$, ΔP, and $\Delta\dot{P}$, and the total values of $\ddot{\nu}$, obtained for PSRs B1855+09 and B1937+21 when the DE211 and PEP740R ephemerides were substituted for DE200. To facilitate comparisons, the DE200 residuals for PSR B1937+21 (Fig. 5*a*) are plotted again at the top of Figure 6, followed by corresponding plots for the solutions using DE211 and PEP740R. The analogous graphs for

TABLE 3

PARAMETER OFFSETS WITH DIFFERENT EPHEMERIDES OR TIMESCALES, RELATIVE TO DE200 AND TT(BIPM92)[a]

Clock or Ephemeris	$\Delta\alpha$ (mas)	$\Delta\delta$ (mas)	$\Delta\mu_\alpha$ (mas yr^{-1})	$\Delta\mu_\delta$ (mas yr^{-1})	ΔP (10^{-17} s)	$\Delta\dot{P}$ (10^{-24})	$\ddot{\nu}$ (10^{-27} s^{-3})
PSR B1855+09:							−1.0
DE211	−38.59	−6.68	0.40	0.04	−138	3.1	−0.4
PEP740R	−70.97	183.84	−0.08	0.03	782	−97.1	−1.9
UTC	0.00	0.05	−0.00	−0.02	−14	−2.1	−2.3
AT1	0.00	0.04	−0.02	0.00	114	1.1	−5.7
Uncertainty	0.07	0.12	0.04	0.06	2	0.4	0.9
PSR B1937+21:							13.2
DE211	−31.26	−11.64	0.333	0.083	33.1	0.5	13.8
PEP740R	30.83	103.44	−0.053	0.002	568.9	−22.7	20.1
UTC	0.03	0.02	−0.009	−0.001	2.0	−0.5	9.4
AT1	0.03	0.05	−0.019	−0.014	39.3	0.6	2.1
Uncertainty	0.03	0.06	0.008	0.009	0.2	0.2	0.3

[a] Total values are listed for $\ddot{\nu}$ rather than differences; the first entry for each pulsar in this column is the value obtained with the default reference standards.

PSR B1855+09 are not shown, as they are essentially indistinguishable from the residuals in Figure 5*b*. Table 3 shows that some of the fitted parameter values change by much more than the statistical measurement uncertainties. Offsets $\Delta\alpha$ and $\Delta\delta$ in the fitted positions are primarily a result of slightly different orientations of the underlying coordinate systems, which are known to be uncertain at levels between 10 and 100 mas (see, for example, Backer et al. 1985; Standish et al. 1988). Other significant parameter differences are found, as well. For example, discrepancies in the proper motions show that the coordinate systems of DE200 and DE211 rotate relative to each other by about 0.34 mas yr^{-1}, nearly 40 times our measurement uncertainty for PSR B1937+21. The differences in P and $\dot{P}$ between the DE200 and DE211 solutions are mostly attributable to different masses assumed for the outer planets. Even larger differences in the solution relative to PEP740R arise from its different choice of averaging interval for defining the barycentric unit of time. For all of these reasons, we again call attention to the need for special care when using astrometric and rotational parameters of millisecond pulsars at their full experimental precision.

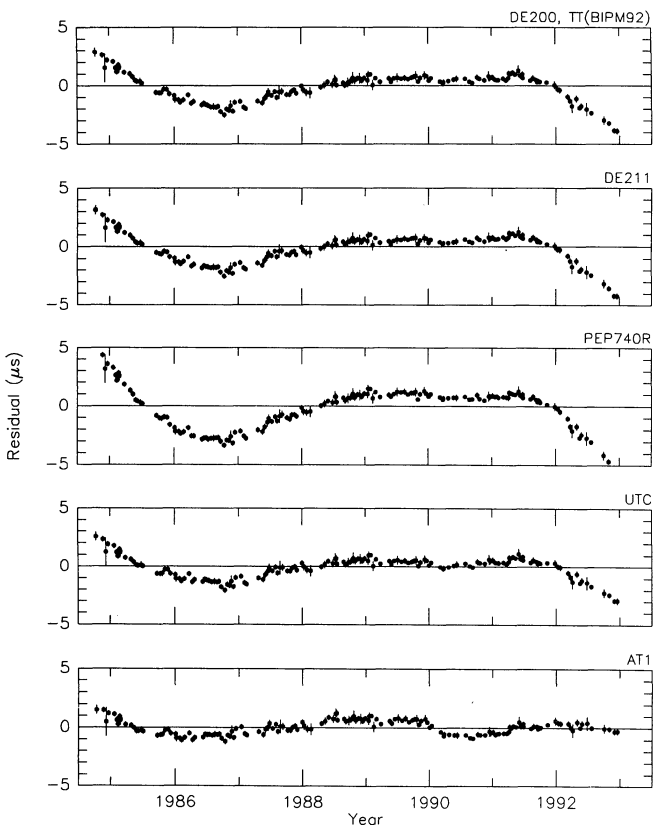

FIG. 6.—Comparison of residuals for different timing solutions for PSR B1937+21. The top panel corresponds to the standard solution with the DE200 ephemeris and TT(BIPM92) timescale (same as Fig. 5*a*); remaining plots illustrate residuals obtained with different ephemerides and timescales.

For our purposes, the most important result of the ephemeris comparisons is that the long-term residual trends (the top three plots in Fig. 6) are very similar to one another, and distinctly different from the flat residuals for PSR B1855+09 seen in Figure 5*b*. Because the two pulsars are separated by only 16° in the sky, ephemeris errors should affect their timing residuals in a similar way. Therefore, if ephemeris errors are responsible for a significant portion of the timing noise in PSR B1937+21, some other deviations must affect the TOAs for PSR B1855+09, and with just the right phase to cancel most of the ephemeris errors. We believe it is much more likely that inaccuracies in the solar system models are not predominantly responsible for the timing noise seen in PSR B1937+21.

6.2. *Atomic Clock Instabilities*

We also carried out solutions to the TOAs for the two pulsars using timescales other than TT(BIPM92). Once again, there are only a few possible choices of reference standards with sufficient accuracy, and the ones we have chosen are not wholly independent. For its ready availability and other good properties we chose UTC as one alternative. We selected AT1, based on free-running clocks maintained at NIST, as a second. Both UTC and TT(BIPM92) derive their frequency calibration and long-term stability mostly from cesium-beam clocks maintained as primary standards at the Physikalish-Technische Bundesanstalt, in Germany (Bauch et al. 1987; Bauch 1990). Therefore, these two timescales are necessarily covariant over intervals exceeding a few months. On the other hand, AT1 is one of many independent, free-running timescales that contribute to determining UTC. Over long intervals it receives relatively low weight in the averages, compared with the PTB

clocks, and thus it remains largely independent of the other standards.

As expected, and confirmed in Table 3 and Figure 6, mostly small differences were found in the fitted pulsar parameters and postfit residuals when UTC was used instead of TT(BIPM92). More significant differences were encountered with respect to AT1, however. When reckoned according to this timescale, the fitted pulsar periods are larger by approximately $\Delta P/P = 2.3 \times 10^{-13}$, and there are also significant differences in $\ddot{\nu}$. These discrepancies are consistent with known rate offsets and suspected instabilities of AT1 relative to the other timescales (D. W. Allan, private communication). The postfit residuals for PSR B1937+21 relative to AT1, shown at the bottom of Figure 6, actually have a smaller variance than those relative to the other timescales. The reverse is true for PSR B1855+09, however, as shown in Figure 7. Furthermore, there is an apparent correlation between the residuals for PSR B1937+21 and PSR B1855+09 when both sets of TOAs are referred to AT1, which indicates clock instabilities dominate in that case. Therefore, we believe that the AT1 timescale is *less* stable than TT(BIPM92), rather than more so; the smaller residuals for PSR B1937+21 almost certainly arise from a partial cancellation of clock drift and another source of low-frequency noise.

6.3. *Interstellar Propagation*

The basic single-pulsar timing model, with constant dispersion measure, leaves postfit residuals for PSR B1937+21 that look significantly different at 1408 and 2380 MHz. In § 4 we interpreted these differences as changes in the column density of free electrons along the line of sight; at some level, such changes must certainly be expected (Armstrong 1984; Blandford, Narayan, & Romani 1984). However, other possibilities also exist for propagation-induced timing fluctuations, with different power-law dependences on observing frequency f. For example, one expects some deviations to be caused by "image wander," the result of refractive wedges in the interstellar medium; or from slightly different free-electron densities along different lines of sight, the latter arising from frequency-dependent scattering effects (Foster & Cordes 1990). Regular observations at three or more observing frequencies could distinguish among these possibilities, at least in principle; already, some timing observations at the much lower frequency of 430 MHz (Cordes et al. 1990) confirm that the bulk of the frequency-dependent changes are very nearly proportional to f^{-2}, as expected for dispersion variations.

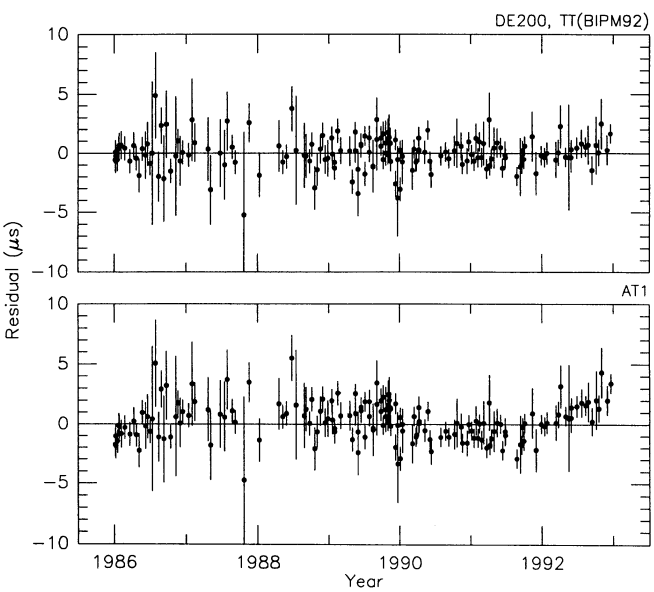

FIG. 7.—Comparison of residuals for different timing solutions for PSR B1855+09. The top panel corresponds to the standard solution with the DE200 ephemeris and TT(BIPM92) timescale (same as Fig. 5*b*); the bottom panel illustrates residuals relative to the AT1 timescale, and shows significant correlated deviations over intervals of several years.

Hu, Romani, & Stinebring (1991) modeled the propagation effects of a two-dimensional phase-perturbing screen with a Kolmogorov spectrum of spatial density irregularities, placed midway between the Earth and PSR B1937+21. They compared the results with timing residuals based on a subset of the present data and found that the slowly varying timing noise cannot be fully explained by frequency-dependent propagation effects. Indeed, they conclude that the bulk of the observed fluctuations of the PSR B1937+21 TOAs (after correction for dispersion-measure changes) is independent of observing frequency. We show in § 7 that the DM variations imply a power-law turbulence index slightly steeper than the Kolmogorov value, but not by enough to significantly alter these conclusions. We therefore believe that our dispersion-corrected TOAs are not seriously contaminated by unmodeled fluctuations in the propagation medium, and that one must look elsewhere for an explanation of the timing irregularities seen in PSR B1937+21.

6.4. *Pulsar Rotational Irregularities*

Although many slow pulsars have timing behavior deviating from a deterministic spin-down law, no millisecond pulsar has yet been shown conclusively to have intrinsic irregularities. For most pulsars the timing-noise amplitude is highly correlated with period derivative (Cordes & Helfand 1980; Cordes & Downs 1985). Arzoumanian et al. (1993) define a stability parameter Δ_8, essentially the base-10 logarithm of typical timing-noise deviations (in seconds) observed over a standard interval of 10^8 s. They show that the relation

$$\Delta_8 = 6.6 + 0.6 \log \dot{P} \qquad (5)$$

characterizes the magnitude of timing noise for most pulsars quite well. The unmodeled fluctuations observed for PSR B1937+21 are close to the magnitude given by this relation, and fully consistent with the scatter (around ± 1 decade) found in its defining plot (Arzoumanian et al. 1994, Fig. 1). Most of the information used to calibrate equation (5) comes from ordinary pulsars with $P > 0.2$ s and $\dot{P} > 10^{-17}$, so its applicability to millisecond pulsars it not well established. But in most other ways the properties of millisecond pulsars are connected smoothly, rather than discontinuously, with those of slow pulsars. It seems entirely reasonable that PSR B1937+21—by a wide margin the youngest and most luminous of field millisecond pulsars—should be the first to exhibit intrinsic timing noise. Thus, by a process of elimination and inference, we are led to the conclusion that our postfit timing residuals for PSR B1937+21 are most likely dominated by its own rotational instability.

6.5. *Cosmic Gravitational Wave Background*

Finally we consider the possibility that low-frequency gravitational waves, perhaps a relic of circumstances in the early universe, might have significant effects on our timing measure-

ments. The basic idea is that the Earth and the subject pulsars are freely falling masses whose positions respond to changes in the local spacetime metric. Passing gravitational waves perturb the metric, inducing changes in the pulse arrival times recorded on Earth. In effect, each line of sight is analogous to one arm of an instrument like LIGO, the proposed Laser Interferometer Gravitational Wave Observatory (Abramovici et al. 1992), with a one-way transmission of highly coherent pulsar pulses replacing the many-times-reflected laser beam. Pulsar timing residuals are most sensitive to gravitational-wave frequencies of order $1/\mathcal{T}$, where $\mathcal{T}$ is the total data span. In units of dimensionless strain, our timing experiment is potentially sensitive to gravitational-wave amplitudes $\delta t/\mathcal{T} \sim 10^{-15}$, where δt is the uncertainty of the measured TOAs. Statistically similar contributions should be expected from metric perturbations occurring at each pulsar and at the Earth. Therefore, for pulsars like PSR B1855+09 and PSR B1937+21 that are close together in the sky, one expects any induced signals to be significantly correlated.

The timing-noise signal in Figure 5*a* can be roughly approximated by a sinusoid with amplitude $A \approx 3$ μs and frequency $f \approx 1/(7\ \mathrm{yr}) \approx 4.5 \times 10^{-9}$ Hz. If such a monochromatic signal were caused by gravitational waves, the energy density in the waves would be

$$\rho = \left(\frac{243\pi^3}{416G}\right) A^2 f^4 \approx 1 \times 10^{-36}\ \mathrm{g\ cm^{-3}} \qquad (6)$$

(see Detweiler 1979; Romani & Taylor 1983). Expressed as a fraction of the closure density of the universe, ρ_c, this result becomes

$$\frac{\rho}{\rho_c} = \frac{8\pi G\rho}{3H_0^2} = 5 \times 10^{-8} h^{-2}\ , \qquad (7)$$

where $H_0 = 100h\ \mathrm{km\ s^{-1}\ Mpc^{-1}}$ is the Hubble constant. Since the amplitude assumed for A was on the high side, and since we observe no similar signal in the data for PSR B1855+09, it would seem very safe to conclude that a continuous-spectrum gravity-wave background cannot have any more than, say 4 times the energy density given by equation (7), per logarithmic frequency interval, at frequencies around 4.5×10^{-9} Hz. In fact, an even tighter limit can be derived by including the PSR B1855+09 data. Using the observations of both pulsars and the statistically rigorous procedure described in Appendix A, we obtain the firm limit

$$\Omega_g h^2 < 6 \times 10^{-8} \quad (95\%\ \text{confidence})\ . \qquad (8)$$

Cosmological models that produce larger gravitational-wave background can be ruled out with high confidence.

7. DENSITY IRREGULARITIES IN THE INTERSTELLAR MEDIUM

The dispersion-measure variations illustrated in Figure 3 can be used to place experimental constraints on small-scale irregularities in the distribution of interstellar free electrons. A standard approach (see, for example, Rickett 1990; Cordes et al. 1990; Narayan 1992) is to model the spectrum of electron-density fluctuations as a power law,

$$P(q) \propto q^{-\beta}\ , \qquad (9)$$

where q represents spatial frequency. The power law arises from the turbulent cascade of energy from lower to higher spatial frequencies, and theory suggests that the index β is likely to be close to the Kolmogorov value for turbulence in neutral gases, 11/3. The spectrum $P(q)$ can be measured using the two-point structure function of phase deviations of the pulsar signal, $D_\phi(b)$, where $b = 2\pi/q$ measures spatial displacements normal to the line of sight. Relative transverse motion of the intervening medium at speed v transforms spatial structure into time variations, according to $b = v\tau$. With a power-law spectrum of density irregularities one expects a phase structure function that is a power law in τ.

$$D_\phi(\tau) = \left(\frac{\tau}{\tau_0}\right)^{\beta-2}\ , \qquad (10)$$

at least over the range of τ corresponding to the domain of applicability of equation (9). If this range extends down to the pulsar's diffractive scintillation timescale τ_d, the theory predicts the normalization condition $\tau_0 = \tau_d$ (Rickett 1977).

The linear relation between phase delay and dispersion measure means that $D_\phi(\tau)$ can be determined from a time series of dispersion-measure variations, DM(t). Over time intervals τ large enough for typical changes in DM to exceed the measurement uncertainties, a good approximation to $D_\phi(\tau)$ is the observable quantity

$$\hat{D}_\phi(\tau) = \left(\frac{2\pi}{f}\,\frac{\mathrm{Hz}}{2.410 \times 10^{-16}\ \mathrm{cm^{-3}\ pc}}\right)^2 \times \langle[\mathrm{DM}(t+\tau) - \mathrm{DM}(t)]^2\rangle\ , \qquad (11)$$

where the angle brackets imply averaging over t. Figure 8 illustrates values of $\hat{D}_\phi$ computed in this way for PSR B1937+21. The phase values refer to observing frequency $f = 1408$ MHz, and the time intervals extend up to $\tau = 2300$ days, about three-fourths of our data span. We fitted the

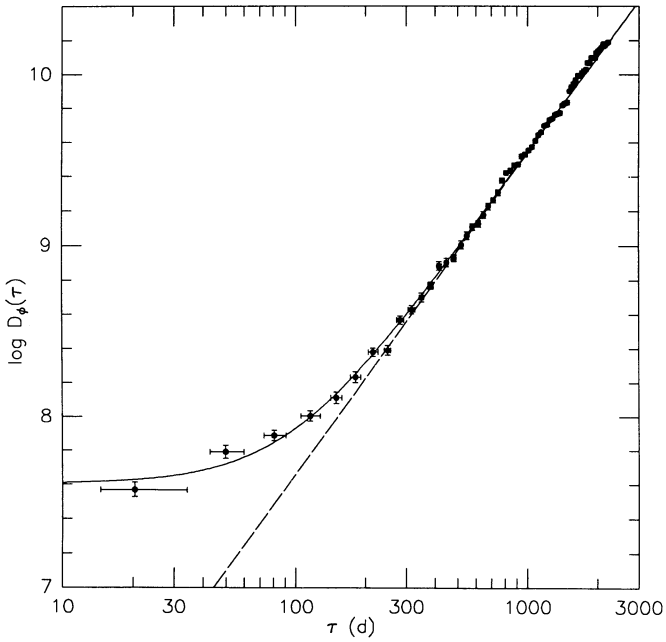

FIG. 8.—Phase structure function $D_\phi(\tau)$ at 1408 MHz, computed from the dispersion-measure variations of PSR B1937+21 (Fig. 3). The fitted curve (*solid line*) corresponds to eq. (12), and the dashed line to eq. (10).

logarithms of measured values of $\hat{D}_\phi$ to the function

$$\log \hat{D}_\phi(\tau) = \log\left[\epsilon + \left(\frac{\tau}{\tau_0}\right)^{\beta-2}\right], \quad (12)$$

where ϵ accounts for the random measurement errors and τ_0 is the time lag at which the noise-corrected phase structure function D_ϕ would be equal to unity. The fitted parameters are

$$\log \epsilon = 7.61 \pm 0.02 ,$$
$$\beta = 3.874 \pm 0.011 ,$$
$$\tau_0 = 11.7 \pm 0.7 \text{ minutes} . \quad (13)$$

and the corresponding functions defined by equations (10) and (12) are plotted as the dashed and solid lines in Figure 8. We note that the uncertainties in the above parameters are likely to be slight underestimates, because only a single realization of the structure function at the longest lag is available.

Our measurement of β exceeds the Kolmogorov value by some 19 standard deviations and is in good agreement with the mean value measured by the same method, over several different lines of sight, by Phillips & Wolszczan (1991). Using the scaling of diffractive scintillation bandwidths measured between 430 and 1400 MHz, Cordes et al. (1990) inferred a somewhat smaller value for PSR B1937+21, namely $\beta = 3.55 \pm 0.11$. Because scintillation bandwidths are difficult to measure, their quoted uncertainty is rather large; moreover, both their uncertainty and ours attempt to account only for random effects. We therefore do not view the discrepancy as serious. The spectral index $\beta = 4$ is a critical value in scintillation theory; values steeper than 4 have been proposed (Blandford & Narayan 1985) to explain various observed phenomena including large intensity modulation indexes, quasi-periodicities in pulsar dynamic spectra, and occasional dramatic radio flux enhancements or "extreme scattering events" (Fiedler et al. 1987). Observations of PSR B1937+21 at Nançay have been interpreted as revealing such an event, occurring over 15 days in 1989 October (Cognard et al. 1993). Our data are too sparsely sampled to provide direct corroborative evidence for their observation; however, our measurement of β is less than 4 by about 11 standard deviations, which implies that in general, the interstellar medium between PSR B1937+21 and the Earth should not support strong focusing.

Another important issue in scintillation theory is the range of spatial frequencies q over which equation (9) remains valid. Dissipation mechanisms are expected to truncate the turbulent energy cascade above some spatial frequency $q_i = 2\pi/l_i$, where the length l_i is often called the "inner scale." Other damping mechanisms, including second-order Fermi acceleration of cosmic rays, are expected to absorb energy at very low spatial frequencies corresponding to length scales greater than some "outer scale," l_0 (see Rickett 1990 and references therein). One can test for the presence of an inner scale, at the same time performing a consistency check of the theory, by comparing values of τ_0 and τ_d measured at the same frequency. These times should be equal if the inner scale is less than the distance the diffracting screen moves in time τ_d, that is, $l_i < v\tau_d$. The diffractive timescale can be obtained from the two-dimensional autocorrelation function of the pulsar's dynamic spectrum; by convention it is taken to be the half-width of the autocorrelation at $1/e$ of its maximum. Cordes et al. (1990) found $\tau_d = 7.4 \pm 0.5$ minutes, while Ryba (1991) found a mean value 6.4 ± 0.3 minutes, as well as some evidence that τ_d may be variable on timescales of a few years. Our value for τ_0 is less than a factor of 2 larger, which we consider very good agreement in view of the necessary extrapolation over more than four decades. Our data thus provide evidence that if an inner scale exists, its value is bounded by

$$l_i < 2 \times 10^9 \left(\frac{v}{50 \text{ km s}^{-1}}\right) \text{ cm} . \quad (14)$$

This limit is in good agreement with the results of Kaspi & Stinebring (1992), who found no evidence for inner scales greater than 10^9 cm, on the basis of long-term refractive scintillation observations for 12 pulsars. Although Gupta, Rickett, & Coles (1993) did find evidence for inner scales greater than 10^9 cm, it came mainly from nearby pulsars having only moderate levels of scattering; we do not consider our results for this much more distant pulsar, in the galactic plane, to be inconsistent with their conclusions. At the opposite end of the length spectrum, our observed power-law dependence $D_\phi(\tau)$ extends to at least $\tau = 2300$ days (see Fig. 8). Therefore the outer scale length must obey the constraint

$$l_o > 1 \times 10^{15} \left(\frac{v}{50 \text{ km s}^{-1}}\right) \text{ cm} . \quad (15)$$

This limit is unsurprising and is much weaker than other measurements which suggest the outer scale length may be as large as parsecs, or even more (Rickett 1990).

8. OTHER CONSEQUENCES OF THE TIMING DATA

We now turn attention to a brief recounting of some other consequences of these observations. We shall discuss, in turn, the distance limits imposed on the two pulsars by their timing parallaxes; the masses and ages of the pulsar and unseen companion in the PSR B1855+09 system; and a limit on the variability of the Newtonian constant of gravity, G. These topics have all been discussed in the literature before, so our updated accounts of the results will be brief.

8.1. *Pulsar Distances*

Pulsar timing measurements are sensitive to annual parallax only through a second-order effect, the small difference in shape between incoming spherical wavefronts and their tangential plane-wave approximations. The resulting signal imposed on TOAs has amplitude $a^2 \cos\beta/2c\,d$, where a is the Earth-Sun distance, β the ecliptic latitide, and d the pulsar distance. For $d = 1$ kpc the maximum amplitude is only 1.2 μs, which helps to explain why PSR B1855+09 remains the only pulsar for which a reliable, nonzero parallax has been obtained from timing observations. Our present data set yields some improvement in accuracy over that presented in Paper I; we now obtain $\pi = 1.1 \pm 0.3$ mas, corresponding to a distance $d = 0.9^{+0.4}_{-0.2}$ kpc. Despite the much better timing accuracy possible for PSR B1937+21, the signature of annual parallax is barely visible in its TOAs, if at all. The nominal 2 σ upper bound is $\pi < 0.28$ mas, corresponding to a distance limit $d > 3.6$ kpc. The dispersion measures of PSR B1855+09 and PSR B1937+21, together with the Taylor & Cordes (1993) model for the distribution of interstellar free electrons, imply respective distances of about 0.7 and 3.6 kpc, with uncertainties of order 25%. The dispersion-based distances and the parallax measurements are thus in satisfactory agreement.

8.2. *Masses and Ages in the PSR B1855+09 System*

The orbital parameters derived for B1855+09 are nearly the same as those obtained in Paper I. They are not affected significantly by any plausible errors in the adopted solar system ephemeris or reference timescale. The best-fitting value of the post-Keplerian parameter r is slightly larger than before, and s is slightly smaller, but the uncertainty ranges overlap satisfactorily (compare Fig. 4 with Fig. 7 of Paper I). According to general relativity, our measured value of r implies a companion mass

$$m_2 = rc^3/G = 0.258^{+0.028}_{-0.016}\ M_\odot\ , \tag{16}$$

which, combined with the mass function (eq. [7] of Paper I) yields

$$m_1 = 1.50^{+0.26}_{-0.14}\ M_\odot \tag{17}$$

for the pulsar mass. Like all other neutron stars with reliable mass estimates (Thorsett et al. 1993), PSR B1855+09 appears to have a gravitational mass close to the Chandrasekhar limit.

Our improved distance and mass estimates will allow somewhat tighter constraints on evolutionary models of the PSR B1855+09 system. Whether this millisecond pulsar was formed by "recycling" a slow pulsar or by accretion-induced collapse of a massive white dwarf, the pulsar must be older than the companion in its present state. Therefore, if an age estimate for the companion can be obtained from cooling models, it provides a lower limit to the neutron star's age. Kulkarni, Djorgovski, & Klemola (1991) studied the PSR B1855+09 field in detail, and concluded that no companion is visible to limiting magnitudes $R > 24.6$ and $I > 23.4$. Our improved distance measurement is very close to the 0.8 kpc value they used for estimating a cooling age for the white dwarf companion. An updated calculation shows that the companion must be older than about 4 Gyr; such an age is consistent with the pulsar's characteristic spin-down age, $P/2\dot{P} = 5$ Gyr, and shows that the pulsar's dipole magnetic field cannot have been decaying exponentially on any timescale less than about 0.4 Gyr.

8.3. *Time Variation of G*

Dirac (1937) suggested that there may be deep theoretical significance in the degree of constancy of Newton's gravitational coupling parameter G. One way to test for changes in G is to compare the observed stabilities of binary-pulsar orbital periods with theoretical expectations. Damour, Gibbons, & Taylor (1988) showed that the appropriate phenomenological limit is

$$\frac{\dot{G}}{G} = -\frac{\delta\dot{P}_b}{2P_b}\ , \tag{18}$$

where $\delta\dot{P}_b$ represents whatever part of the observed orbital period derivative that is not otherwise explained (e.g., by gravitational radiation damping). The best current experimental limit of this kind, derived from data for PSR B1913+16 (Taylor 1993), yields

$$\frac{\dot{G}}{G} = (4 \pm 5) \times 10^{-12}\ \mathrm{yr}^{-1} \quad \text{(PSR B1913 + 16)}\ . \tag{19}$$

Precise interpretation of the limit depends on the poorly known equation of state for bulk nuclear matter, with "softer" equations yielding somewhat weaker limits (Nordtvedt 1990). The new measurement of $\dot{P}_b$ for PSR B1855+09 listed in Table 2 yields a slightly weaker phenomenological limit,

$$\frac{\dot{G}}{G} = (-9 \pm 18) \times 10^{-12}\ \mathrm{yr}^{-1} \quad \text{(PSR B1855+09)}\ . \tag{20}$$

In this case the interpretation is more secure because the orbiting companion is not a neutron star. With continued observations, the limit from PSR B1855+09 should improve as $\mathcal{T}^{-2.5}$, with an ultimate precision (perhaps limited by unknown galactic accelerations, see Damour & Taylor 1991) at least an order of magnitude below the present limit.

9. FEASIBILITY OF A PULSAR TIMESCALE

We have shown that timing residuals for PSRs B1855+09 and B1937+21 have fractional amplitudes $\delta t/\mathcal{T} \sim 10^{-14}$, comparable to the estimated long-term stabilities of the best atomic clocks. Clock stabilities are customarily analyzed by fitting and removing a linear phase drift and performing a spectral analysis of the remaining fractional frequency differences, or, equivalently, by measuring the variances of second differences in the time domain over a sequence of time intervals (Rutman & Walls 1991; Percival 1991). Because pulsar timing residuals already have a second-order polynomial removed, their long-term stabilities are not best characterized by these same statistical measures. Instead, suitable stability measures involve spectral analysis of the *drift rates* of fractional frequency differences, or the variance of *third* differences of residuals at specified time intervals.

Taylor (1991) proposed the use of a dimensionless fractional instability called σ_z, a logical extension of the Allan variance used in the clock community, and well suited for characterizing the stability of pulsar TOAs as well as man-made clocks and time series of other kinds. It is defined by the relation

$$\sigma_z^2(t) = (m/\mathcal{T})^3 S_m\ , \tag{21}$$

where $t = \mathcal{T}/m$ and S_m is a power spectral density estimate obtained by fitting orthonormal polynomials to a sequence of clock differences (Stinebring et al. 1990; see also Appendix A). The timing residuals in Figure 5 yield the values of σ_z plotted in Figure 9. For PSR B1855+09 the measurements are well approximated by a straight line with slope $-3/2$, as expected whenever random measurement errors dominate. For PSR B1937+21, however, low-frequency noise causes the observed values of σ_z to turn upward at $t \approx 2$ yr. The spectral slope at the longest timescales is not well determined by the data, although it is consistent with values between about 0.5 and 2 that are characteristic of many slow pulsars with intrinsic timing noise.

It has been suggested that a pulsar-based timescale might be feasible, and that it could be useful for establishing a long-term standard of frequency and time (Taylor 1991; Petit, Tavella, & Thomas 1992). Pulsars are like flywheels: their present rates of rotation are determined by complicated evolutionary circumstances, rather than by fundamental constants of nature like the atomic energy-level differences that regulate the behavior of atomic clocks. For this reason it would not make sense to define the length of the second in terms of pulsar observations. Nevertheless, if a number of millisecond pulsars are observed regularly for many years, as we and others are now doing, it should be possible to establish an ensemble-average pulsar timescale through a suitable stability algorithm. Such a timescale might have better long-term stability than existing atomic

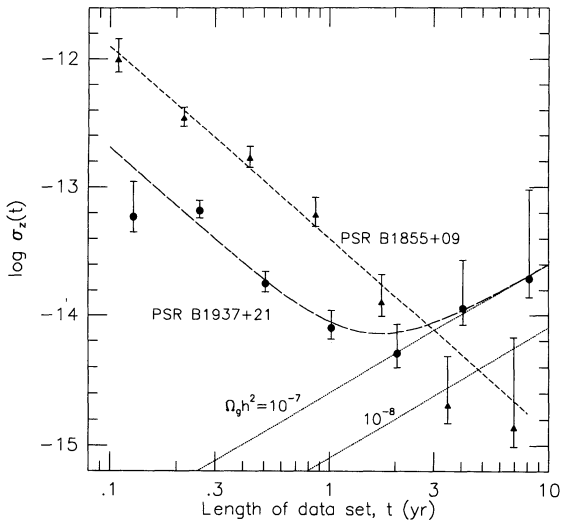

FIG. 9.—Fractional instabilities $\sigma_z(t)$ of PSRs B1855+09 and B1937+21. The fitted curves have slopes of $-3/2$ for values of t small enough that measurement errors dominate. For PSR B1937+21, some other source of noise is evidently present at $t \gtrsim 2$ yr; the suggested fit includes a second power-law term with slope +1. For comparison, the dotted lines illustrate the noise contribution corresponding to hypothetical cosmic gravitational-wave backgrounds of energy density $\Omega_g h^2 = 10^{-7}$ and 10^{-8}, according to eqs. (A5) and (21).

time standards and would be highly valuable for use in establishing the relative instabilities of different realizations of terrestrial time.

10. SUMMARY AND PROSPECTS

More than a decade of effort has gone into acquiring the data and results we have presented, and it is gratifying to see this work continuing to produce unique and interesting results. Our timing measurements have a fractional accuracy that places them among the most precise ever made, by any technique. Similar comments apply to the astrometric, stellar rotation, interstellar dispersion, and orbital parameters that are extracted from the data. We have used general relativity as an astrophysical tool in determining the masses of PSR B1855+09 and its companion, thereby providing basic data that will be useful in stellar evolution applications—especially when combined with our improved distance estimate. Tight limits are placed on the variability of Newton's gravitational constant, and propagation effects are used to place new constraints on the nature of the interstellar medium.

Extensive efforts to identify the source of low-amplitude, low-frequency timing noise in PSR B1937+21 strongly suggest that the pulsar itself is responsible. To help us reach this conclusion we have, for the first time, effectively timed one pulsar against another. Even if it is true that an intrinsic instability has been found in PSR B1937+21, it appears likely that older millisecond pulsars with smaller period derivatives, including PSR B1855+09, will have proportionally smaller intrinsic timing noise. Many additional millisecond pulsars (including PSRs J0437−4715, B1257+12, B1534+12, J1713+0747, J2019+2425, J2229+26, J2235+1506, J2317+1439, and J2322+2057) have been found in the past 2–3 yr and have characteristics suitable for high-precision timing measurements similar to those described here. We therefore believe that excellent prospects exist for continuation of the rich lode of information uncovered whenever high-precision timing measurements of fast pulsars are made.

We are deeply indebted to many colleagues who have contributed to this project in the past, including D. Backer, M. Davis, L. Rawley, D. Stinebring, and J. Weisberg, and to the highly skilled and dedicated telescope operators at Arecibo, especially A. Vázquez, who have made most of the observations. Our work is supported by the US National Science Foundation under grant AST 91-15103, and V. M. K. received additional support from the National Science and Engineering Research Council of Canada. Arecibo Observatory is operated by Cornell University, under a cooperative agreement with the NSF.

APPENDIX A

RIGOROUS LIMIT ON A GRAVITATIONAL-WAVE BACKGROUND

Cosmological models suggest that during the radiation-dominated era in the early universe, a fixed fraction of the energy within a horizon scale should be channeled in a self-similar way into gravitational radiation with comoving wavelength a constant fraction of the horizon size (Bertotti, Carr, & Rees 1983; Blandford et al. 1984; Hogan & Rees 1984; Witten 1984). As a consequence Ω_g, the fractional energy density in gravitational waves per logarithmic frequency interval, is expected to be independent of frequency. Under these conditions the power spectrum of pulsar timing residuals, if dominated by the influence of a gravitational-wave background (GWB), is given by

$$P_g(f) = \frac{H_0^2}{8\pi^4}\,\Omega_g f^{-5}\,. \tag{A1}$$

With the frequency f measured in cycles per year, the residuals in microseconds, and a Hubble constant $H_0 = 100h$ km s^{-1} Mpc^{-1}, the spectrum may be written as

$$P_g(f) = 1.34 \times 10^4 \Omega_g h^2 f^{-5}\ \mu\text{s}^2\ \text{yr}\,. \tag{A2}$$

Detecting this steep power-law signal, or determining a rigorous upper bound, is obviously an important cosmological goal.

Our procedure for setting a bound on $\Omega_g h^2$ begins by performing a low-resolution spectral analysis of one or more sets of pulsar timing residuals, using the technique of Stinebring et al. (1990). The method uses orthonormal polynomials as basis functions and produces reliable spectra spanning many octaves, with good rejection of frequency components below each analyzed band (Groth

1975; Deeter 1984). Spectral estimates are computed by using a Gram-Schmidt procedure to find the coefficients of a set of polynomials p_j of order $j = 0, 1, 2, 3$, defined so as to be orthonormal over the available TOAs. A least-squares fit of the four polynomials to a set of residuals $R(t_i)$, $i = 1, N$, yields the values of constants C_j that minimize the sum

$$\chi^2 = \sum_{i=1}^{N} \left[R(t_i) - \sum_{j=0}^{3} C_j p_j(t_i) \right]^2 . \tag{A3}$$

The first three C_j's are fully covariant with the fitted parameters ϕ_0, ν, and $\dot{\nu}$ (see eqs. [1] and [2]), and therefore contain no additional information about the pulsar's timing stability. However, the square of C_3 provides an estimate, S_1, of the spectral power density in a one-octave band near the lowest accessible frequency, $f \approx 1/\mathcal{T}$. The sequence of residuals is then divided into m subsequences of approximately equal duration, starting with $m = 2$. The χ^2 minimization is repeated for each subsequence, yielding m new values of C_3 whose mean square provides an additional spectral density estimate, S_m, corresponding to fluctuation power at frequencies near $f = m/\mathcal{T}$. Further subdivisions yield additional spectral estimates S_m, $m = 4, 8, \ldots$, for similarly shaped frequency bands spaced by one-octave steps. Table 4 lists the first four S_m's computed in this way for the two data sets illustrated in Figure 5.

We assume that several sources of noise may contribute to the observed spectral densities. There will certainly be a "white" spectral component, independent of frequency, arising from the uncorrelated measurement errors of the TOAs. One or more "red" components may also be present, with increasing spectral densities toward lower frequencies. Such contributions might arise from any of the sources discussed in § 6, including a stochastic GWB. To obtain a rigorous limit on $\Omega_g h^2$—that is, an upper bound on the contribution to observed S_m's from the red-noise source defined in equation (A2)—we need to calculate the joint probability of having measured a set of spectral coefficients as small as those actually observed, or smaller, in the presence of the known measurement noise, a specified energy density in the GWB, and possibly other noise sources of unspecified origin.

Whatever the contributions to the underlying noise, each of the measured values of S_m is a random variable having a χ^2 distribution with m degrees of freedom; its expectation value is equal to the average (over many statistical realizations) of the sum of all noise contributions. For an assumed GWB these averages can be estimated by Monte Carlo simulation, using random power-law data sampled at the same t_i's as the actual data sets (Stinebring et al. 1990). This procedure effectively serves to calibrate the "gain" of the octave-bandwidth spectral filter represented by each S_m. In Table 4 we list separately the simulated expectation values $\langle S_m \rangle_w$, for the known amounts of white measurement noise, and $\langle S_m \rangle_g$, for a hypothetical GWB with $\Omega_g h^2 = 10^{-7}$. The total expectation value for a particular S_m is obtained by adding the white-noise and GWB contributions,

$$\langle S_m \rangle = \langle S_m \rangle_w + \langle S_m \rangle_g , \tag{A4}$$

with linear scaling of the second term for assumed values of $\Omega_g h^2$ other than 10^{-7}. We note in passing that for approximately uniform sampling, the simulated expectation values for the GWB component are well approximated by the simple expression

$$\langle S_m \rangle_g \approx 6.6 \times 10^4 \Omega_g h^2 f^{-5} \ \mu\text{s}^2 \ \text{yr} , \tag{A5}$$

with $f = m/\mathcal{T}$ measured in cycles per year.

With m degrees of freedom and a χ^2 distribution, the cumulative probability of an experimental outcome being less than x times the expectation value is given by the incomplete gamma function $P(m/2, mx/2)$ (see, for example, Press et al. 1986). In this language, each of our measurements S_m represents an experimental outcome; however, we want to know not its a priori probability when compared to $\langle S_m \rangle$, but rather a value normalized by the probability of obtaining the same measurement if only white noise were present, i.e., if the expectation value were $\langle S_m \rangle_w$. For the jth entry in a table of measurements of S_m, the normalized probability can be written

$$\mathcal{P}_j = \frac{P(m/2,\ xm/2)}{P(m/2,\ ym/2)} , \tag{A6}$$

where

$$x = \frac{S_m}{\langle S_m \rangle_w + \langle S_m \rangle_g} , \tag{A7}$$

TABLE 4

OBSERVED AND COMPUTED SPECTRAL DENSITIES OF PULSAR TIMING RESIDUALS[a]

PSR	j	m	f (yr^{-1})	S_m (μs^2 yr)	$\langle S_m \rangle_w$ (μs^2 yr)	$\langle S_m \rangle_g$ (μs^2 yr)
B1937+21	1	1	0.12	207	0.087	238
	2	2	0.24	8.84	0.071	8.03
	3	4	0.49	0.218	0.071	0.242
	4	8	0.98	0.067	0.071	0.008
B1855+09	5	1	0.14	0.622	3.08	112
	6	2	0.29	0.170	3.68	4.32
	7	4	0.58	0.824	2.53	0.23
	8	8	1.15	2.37	2.37	0.059

[a] Values of $\langle S_m \rangle_g$ correspond to an assumed gravitational-wave background with $\Omega_g h^2 = 10^{-7}$.

$$y = \frac{S_m}{\langle S_m \rangle_w} . \tag{A8}$$

Note that $\mathscr{P}_j \approx 1$ whenever $\langle S_m \rangle_g \ll \langle S_m \rangle_w$, which has the desired result of effectively removing from consideration any spectral estimates S_m with negligible expected contribution from the GWB.

Because the individual values of S_m are statistically independent, the normalized total probability of having measured an entire set as small as the observed ones, in the presence of the specified GWB, is

$$\mathscr{P}_t = \prod_j \mathscr{P}_j . \tag{A9}$$

The complement of $\mathscr{P}_t$ is equal to the confidence with which one can reject the value of $\Omega_g h^2$ used for the simulation of $\langle S_m \rangle_g$. A plot of GWB upper bounds as a function of $\mathscr{P}_t$ is presented in Figure 10, with separate lines drawn for the product in equation (A9) taken over the measurements for each pulsar alone, as well as over all of the measurements. The combined data for both pulsars provide the rigorous limits

$$\begin{aligned} \Omega_g h^2 &< 1.4 \times 10^{-8} \quad \text{(68\% confidence)} \\ \Omega_g h^2 &< 6 \times 10^{-8} \quad \text{(95\% confidence)} \\ \Omega_g h^2 &< 1 \times 10^{-7} \quad \text{(99\% confidence)} \end{aligned} \tag{A10}$$

on the stochastic GWB. These are the best current limits on such radiation, and they may be used to evaluate any cosmological model that has been worked out in sufficient detail to predict a gravity-wave background.

A better appreciation of the experimental basis of our GWB limit can be gained by studying Figure 9. In this graph the residual spectral densities S_m have been converted to dimensionless instabilities, $\sigma_z(t)$, according to equation (21). A similar conversion of the theoretical spectra for $\Omega_g h^2 = 10^{-7}$ and 10^{-8}, using equation (A5), yields the dotted straight lines in the figure, with slope $+1$. The values of $\sigma_z(t)$ for PSR B1855+09 at $t = 3.5$ yr and $t = 7.0$ yr lie well below these lines and are primarily responsible for the tight limits quoted in equation (A10).

APPENDIX B

ARCHIVAL STORAGE OF PULSAR TIMING DATA

Our observations will be of interest to others working on related topics including astrometry, celestial reference frames, neutron-star physics, solar system dynamics, and timekeeping metrology. Moreover, we believe it is highly desirable for pulsar TOAs to be archived and made available for analysis in combination with other measurements, both now and in the future. To this end we have drafted some general guidelines for an "Interchange TOA" (ITOA) format for pulse arrival times, and we have used it to create an archive with our own data for PSR B1855+09 and PSR B1937+21. The resulting plain-text ASCII files are freely available by anonymous ftp over Internet.

Each archival file begins with a free-format header describing the data. For the ITOA files, this description includes the precise coordinates of the observatory, which will be needed for most applications of the data, as well as information concerning the reference timescale, data acquisition systems, and so on. As illustrated by the file fragment reproduced in Table 5, the header section of an ITOA file is terminated by an underlined list of column headings identifying the remaining data in the file. After the headings come the tabular data itself, with a single line for each measured TOA. Successive columns contain pulsar name, the TOA expressed as a Modified Julian Date (MJD ≡ JD − 2400000.5), estimated uncertainty of the TOA in microseconds, topocentric observing frequency, dispersion-measure correction, coded observatory name, and a comment field. We define the tabulated dispersion-

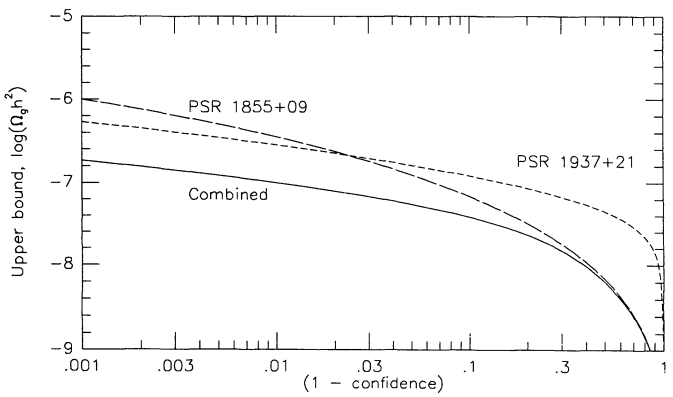

FIG. 10.—Upper bound for $\Omega_g h^2$, the fractional energy density of a gravitational-wave background, plotted as a function of confidence level. The solid line is a combined limit based on measurements of both PSRs B1855+09 and B1937+21.

TABLE 5

THE FIRST FEW LINES OF AN INTERCHANGE-FORMAT ARCHIVAL TOA FILE

Topocentric TOA: for PSR B1937+21 at Arecibo Observatory (AO)
XYZ coordinates (m): 2390490 −5564764 1994727 Reference clock: UTC
Observing systems:
mk2_14 (System A): Mark II, 1408 MHz, 0.25 MHz filter bank
mk2_23 (System B): Mark II, 2380 MHz, 0.25 MHz filter bank
mk3_14m (System C): Mark III, 1408 MHz, 0.25 MHz filter bank
mk3_14r (System E): Mark III, 1408 MHz, coherent de-dispersers
mk3_23m (System F): Mark III, 2380 MHz, 0.25 MHz filter bank
Notes: 8.68 μs added to all System A, C, TOAs
3.91 μs added to all System E TOAs
Reference: Kaspi, Taylor, & Ryba. 1993, ApJ (submitted).

PSR	TOA (MJD)	err (μs)	freq (MHz)	Del_DM (cm-3 pc)	obs	Comments
1937+21	47541.6553241012920	0.34	2385.0000	0.000926	AO	mk3_23m
1937+21	47544.6493692046961	0.32	2370.0000	0.000926	AO	mk3_23m
1937+21	47556.6127951448270	0.16	2375.0000	0.000793	AO	mk3_23m
1937+21	47586.5384895827892	0.14	2390.0000	0.000588	AO	mk3_23m
1937+21	47613.4636053418367	0.14	2380.0000	0.000456	AO	mk3_23m
1937+21	47664.3211284840220	0.22	2365.0000	0.000197	AO	mk3_23m
1937+21	47676.2957812637231	0.20	2375.0000	0.000232	AO	mk3_23m
...						

measure corrections as increments to be added to a pulsar's nominal DM to obtain more accurate values which track measured changes in the interstellar medium. For observatory identifications we suggest using a two-letter code, e.g., AO for Arecibo, GB for Green Bank, JB for Jodrell Bank, NC for Nançay, PK for Parkes, etc.

The ITOA format specifies no fixed number of characters for each data field. Instead the fields are separated by one or more blank spaces to align them vertically, and zeros are inserted in place of unavailable information (e.g., dispersion-measure corrections in our file for PSR B1855+09). We call special attention to the fact that in order to avoid degrading the experimental precision, listed TOAs require five decimal digits for the Modified Julian Day number and about 13 for the fractional part of a day. Because of this total of 18 digits exceeds the precision of commonly used 64 bit floating-point representations, extra programming care must be exercised when manipulating TOAs as numbers. We generally read and store the integer and fractional parts of these numbers separately, and we design the related high-precision algorithms accordingly.

For those whose primary interest is in the postfit timing residuals rather than the raw TOAs, we have also defined an "Interchange Residual" (IRES) format, an example of which is excerpted in Table 6. Like the ITOA files, the IRES files also begin with a free-format header describing the file. Relevant header information will typically include the pulsar name, name and version number of the program used to calculate the residuals, reference timescale and ephemeris, observatory coordinates, and assumed

TABLE 6

THE FIRST FEW LINES OF AN INTERCHANGE-FORMAT ARCHIVAL RESIDUAL FILE

PSR B1937+21 residuals TEMPO v9.035 Clock: UTC Ephemeris: DE200
Arecibo XYZ coordinates (m): 2390490, −5564764, 1994727
RA (J2000): 193938.560210 DEC (J2000): 213459.14166
Proper Motion (mas/yr) RA: −0.130 DEC: −0.464
P (s): 0.001557806468819778 Pdot (10^-15): 0.0001051189
Epoch (MJD): 47500.0000 Parallax (mas): 0.25
Dispersion Measure (pc cm^-3): 71.040 + Del_DM
Observing systems:
mk2_14 (System A): Mark II, 1408 MHz, 0.25 MHz filter bank
mk2_23 (System B): Mark II, 2380 MHz, 0.25 MHz filter bank
mk3_14m (System C): Mark III, 1408 MHz, 0.25 MHz filter bank
mk3_14r (System E): Mark III, 1408 MHz, coherent de-dispersers
mk3_23m (System F): Mark III, 2380 MHz, 0.25 MHz filter bank
Reference: Kaspi, Taylor, & Ryba. 1993, ApJ (submitted).

TOA_bry (MJD)	resid (μs)	err (μs)	freq_bry (MHz)	Del_DM (cm-3 pc)	phase	obs	comments
47541.6518	0.686	0.34	2385.0196	0.000926	0.0000	AO	mk3_23m
47544.6458	1.126	0.32	2370.0103	0.000926	0.0000	AO	mk3_23m
47556.6093	1.207	0.16	2374.9734	0.000793	0.0000	AO	mk3_23m
47586.5358	0.925	0.14	2389.8897	0.000588	0.0000	AO	mk3_23m
47613.4625	0.549	0.14	2379.8407	0.000456	0.0000	AO	mk3_23m
47664.3236	0.764	0.22	2364.8436	0.000197	0.0000	AO	mk3_23m
47676.2990	0.456	0.20	2374.8611	0.000232	0.0000	AO	mk3_23m
...							

pulsar parameters. Again the header section is terminated by an underlined sequence of column headings. Columns of tabular data follow, presenting for each measurement the equivalent barycentric TOA, residual and measurement uncertainty in microseconds, barycentric observing frequency, dispersion-measure correction, orbital phase, observatory code, and a comment field. We emphasize that while TOAs and clock corrections, once archived, are fixed and should not change, residuals depend on numerous details of the fitted model including ephemeris, reference timescale, parameter values, and weights assigned to the data.

To obtain the ITOA and IRES files over Internet, you should log onto a network-ready computer and enter commands similar to the following:

```
% ftp pulsar.princeton.edu      (or ftp 128.112.84.73)
Name: anonymous
Password: yourname@your.address.edu
ftp> cd pub/toa
ftp> get READ.ME
ftp> mget *.92*
ftp> quit
% ...
```

The file named READ.ME contains further details on the format and contents of the archive files as well as a log of significant changes and updates. The presently available files contain Arecibo Observatory data through 1992 December and include 1885ao.92t, 1855ao.92r, 1937ao.92t, and 1937ao.92r, the suffixes t and r denoting TOAs and residuals, respectively. A version of our pulsar timing software package TEMPO, able to read and write interchange-format TOAs, is also available. It and related documentation are located in the pub/tempo directory.

REFERENCES

Abramovici, A., et al. 1992, Science, 256, 325
Armstrong, J. W. 1984, Nature, 307, 527
Arzoumanian, Z., Nice, D. J., Taylor, J. H., & Thorsett, S. E. 1994, ApJ, 422, 621
Backer, D. C., Fomalont, E. B., Goss, W. M., Taylor, J. H., & Weisberg, J. M. 1985, AJ, 90, 2275
Backer, D. C., Kulkarni, S. R., & Taylor, J. H. 1983, Nature, 301, 314
Bauch, A. 1990, in Impact of Pulsar Timing on Relativity and Cosmology, ed. D. C. Backer (Berkeley: Center for Particle Astrophysics), b1
Bauch, A., Dorenwendt, K., Fischer, B., Heindorff, T., Müller, E. K., & Schröder, R. 1987, IEEE Trans. Instrum. Meas., IM-36, 613
Bertotti, B., Carr, B. J., & Rees, M. J. 1983, MNRAS, 203, 945
Blandford, R. D., & Narayan, R. 1985, MNRAS, 213, 591
Blandford, R. D., Narayan, R., & Romani, R. W. 1984, J. Astrophys. Astron., 5, 369
Cognard, I., Bourgois, G., Lestrade, J.-F., Biraud, F., Aubry, D., Darchy, D., & Drouhin, J.-P. 1993, Nature, 366, 320
Cordes, J. M., & Downs, G. S. 1985, ApJS, 59, 343
Cordes, J. M., & Helfand, D. J. 1980, ApJ, 239, 640
Cordes, J. M., Wolszczan, A., Dewey, R. J., Blaskiewicz, M., & Stinebring, D. R. 1990, ApJ, 349, 245
Damour, T., & Deruelle, N. 1985, Ann. Inst. H. Poincaré (Physique Théorique), 43, 107
———. 1986, Ann. Inst. H. Poincaré (Physique Théorique), 44, 263
Damour, T., Gibbons, G., & Taylor, J. H. 1988, Phys. Rev. Letters, 61, 1151
Damour, T., & Taylor, J. H. 1991, ApJ, 366, 501
———. 1992, Phys. Rev. D, 45, 1840
Davis, M. M., Taylor, J. H., Weisberg, J. M., & Backer, D. C. 1985, Nature, 315, 547
Deeter, J. 1984, ApJ, 281, 482
Detweiler, S. 1979, ApJ, 234, 1100
Dirac, P. A. M. 1937, Nature, 139, 323
Fairhead, L., Bretagnon, P., & Lestrade, J.-F. 1988, IAU Symp. 128, in The Earth's Rotation and Reference Frames for Geodesy and Geodynamics, ed. A. K. Babcock & G. A. Williams (Dordrecht: Kluwer), 419
Fiedler, R. L., Dennison, B., Johnston, K. J., & Hewish, A. 1987, Nature, 326, 675
Foster, R. S., & Cordes, J. M. 1990, ApJ, 364, 123
Groth, E. J. 1975, ApJS, 29, 443
Guinot, B. 1988, A&A, 192, 370
Guinot, B., & Petit, G. 1990, in Impact of Pulsar Timing on Relativity and Cosmology, ed. D. Backer (Berkeley: Center for Particle Astrophysics), C1
Gupta, Y., Rickett, B. J., & Coles, W. A. 1993, ApJ, 403, 183
Hankins, T. H., Stinebring, D. R., & Rawley, L. A. 1987, ApJ, 315, 149
Hogan, C. J., & Rees, M. J. 1984, Nature, 311, 109
Hu, W., Romani, R. W., & Stinebring, D. R. 1991, ApJ, 366, L33
Kaspi, V. M., & Stinebring, D. R. 1992, ApJ, 392, 530
Kulkarni, S. R., Djorgovski, S., & Klemola, A. R. 1991, ApJ, 367, 221
Narayan, R. 1992, Phil. Trans. R. Soc. Lond., A341, 151
Nordtvedt, K. 1990, Phys. Rev. Letters, 65, 953
Percival, D. B. 1991, Proc. IEEE, 79, 961
Petit, G., Tavella, P., & Thomas, C. 1992, in Proc. 6th European Frequency and Time Forum (ESA SP-340), 57
Phillips, J. A., & Wolszczan, A. 1991, ApJ, 382, L27
Press, W. H., Flannery, B. P., Teukolsky, S. A., & Vetterling, W. T. 1986, Numerical Recipes: The Art of Scientific Computing (Cambridge: Cambridge Univ. Press)
Rawley, L. A. 1986, Ph.D. thesis, Princeton Univ.
Rawley, L. A., Taylor, J. H., & Davis, M. M. 1988, ApJ, 326, 947
Rawley, L. A., Taylor, J. H., Davis, M. M., & Allan, D. W. 1987, Science, 238, 761
Rickett, B. J. 1977, ARA&A, 15, 479
———. 1990, ARA&A, 28, 561
Romani, R. W., & Taylor, J. H. 1983, ApJ, 265, L35
Rutman, R., & Walls, F. L. 1991, Proc. IEEE, 79, 952
Ryba, M. F. 1991, Ph.D. thesis, Princeton Univ.
Ryba, M. F., & Taylor, J. H. 1991a, ApJ, 371, 739 (Paper I)
———. 1991b, ApJ, 380, 557 (Paper II)
Segelstein, D. J., Rawley, L. A., Stinebring, D. R., Fruchter, A. S., & Taylor, J. H. 1986, Nature, 322, 714
Shapiro, I. I. 1964, Phys. Rev. Lett., 13, 789
Standish, E. M. 1982, A&A, 114, 297
———. 1993, AJ, 105, 2000
Standish, E. M., Newhall, X. X., Williams, J. G., & Dickey, J. O. 1988, in IAU Symp. 128, The Earth's Rotation and Reference Frames for Geodesy and Geodynamics, ed. A. K. Babcock & G. A. Wilkins (Dordrecht: Kluwer), 49
Stinebring, D. R., Kaspi, V. M., Nice, D. J., Ryba, M. F., Taylor, J. H., Thorsett, S. E., & Hankins, T. H. 1992, Rev. Sci. Instr., 63, 3551
Stinebring, D. R., Ryba, M. F., Taylor, J. H., & Romani, R. W. 1990, Phys. Rev. Lett., 65, 285
Taylor, J. H. 1991, Proc. IEEE, 79, 1054
———. 1992, Phil. Trans. R. Soc. Lond. A341, 117
———. 1993, in Particle Astrophysics, 4th Rencontres de Blois, ed. J. T. T. Vân, in press
Taylor, J. H., & Cordes, J. M. 1993, ApJ, 411, 674
Taylor, J. H., & Weisberg, J. M. 1989, ApJ, 345, 434
Thorsett, S. E., Arzoumanian, Z., McKinnon, M. M., & Taylor, J. H. 1993, ApJ, 405, L29
Witten, E. 1984, Phys. Rev. D, 30, 272